Elastic fingering patterns in confined lifting flows

João V. Fontana and José A. Miranda*
Departamento de Física, Universidade Federal de Pernambuco, Recife, Pernambuco 50670-901, Brazil
(Received 5 July 2016; published 14 September 2016)

The elastic fingering phenomenon occurs when two confined fluids are brought into contact, and due to a chemical reaction, the interface separating them becomes elastic. We study elastic fingering pattern formation in Newtonian fluids flowing in a lifting (time-dependent gap) Hele-Shaw cell. Using a mode-coupling approach, nonlinear effects induced by the interplay between viscous and elastic forces are investigated and the weakly nonlinear behavior of the fluid-fluid interfacial patterns is analyzed. Our results indicate that the existence of the elastic interface allows the development of unexpected morphological behaviors in such Newtonian fluid flow systems. More specifically, we show that depending on the values of the governing physical parameters, the observed elastic fingering structures are characterized by the occurrence of either finger tip splitting or side branching. The impact of the elastic interface on finger-competition events is also discussed.

DOI: 10.1103/PhysRevE.94.033110

I. INTRODUCTION

The lifting Hele-Shaw cell system is nowadays a broadly studied fluid dynamic problem [1–23]. The continued interest on this particular physical arrangement is, in part, due to its academic importance, related to the formation of viscous fingering interfacial patterns in a confined geometry complementary to the conventional, injection-driven, radial Hele-Shaw cell situation [24–29]. On the practical side, the attractive nature of the lifting Hele-Shaw cell problem resides on the fact that it involves essentially the same experimental setup as the so-called probe-tack test [30,31], a technique widely used to study technologically relevant problems in adhesion science [32–45].

Contrary to the usual injection-driven, radial viscous fingering problem [24–29] which describes the displacement of a more viscous fluid by a less viscous one in a constant-gap Hele-Shaw cell (a device constituted by two parallel glass plates separated by a small distance), the lifting version of the problem considers flow in a variable-gap cell. Specifically speaking, in the lifting case, the cell gap varies with time; i.e., the upper cell plate is lifted parallel to the lower one, while the lower plate is held fixed. As the upper plate is lifted, the outer (less viscous) fluid invades the inner (more viscous) fluid, so that the initially circular fluid-fluid interface retracts, and is destabilized by the Saffman-Taylor, viscous fingering instability [46,47]. As a consequence, small undulations arise at the two-fluid interface. Afterwards, the amplitude of these deformations grows, and finger-shaped structures of the outer fluid evolve, and propagate towards the center of the cell. As time progresses, increasingly complex, visually striking, interfacial fingering patterns are formed [1–23,32–45].

The characteristic shape of the emerging interfacial patterns that arise during lifting Hele-Shaw flows normally depends on the nature of the fluids. If the fluids are Newtonian, one usually observes that the invading fingers increase in length and compete among themselves. These invading fingers present smooth boundaries and only get slightly wider at their tips as time advances. This general behavior is observed in laboratory experiments, as well as in numerical simulations of the lifting flow system [5,12,13,15,20,33]. A completely different pattern-forming scenario is detected experimentally, if the lifted fluid materials are non-Newtonian (e.g., elastic, viscoelastic, viscoplastic fluids, etc.). In such cases, even though the penetrating fingers still compete, the shape of the invading fingers can be considerably convoluted, presenting morphological features like side branching and tip splitting [10,16,17,19].

As discussed in Ref. [48], for Hele-Shaw flows with Newtonian fluids, fingers form structures showing side branching and tip splitting only under very extreme experimental conditions, such as vanishing surface tension or very high lifting velocity or if the lower cell plate is etched [1,24,49]. On the other hand, for Hele-Shaw displacements with non-Newtonian fluids, the rheological properties of the fluids seem to naturally introduce an intrinsic anisotropy into the system, so that fractal-like or dendriticlike aspects such as side branching and tip splitting are more easily produced (see, for instance, Refs. [50–57]).

In this work, we study the phenomenon of elastic fingering in variable-gap Hele-Shaw cells. The occurrence of elastic fingering has already been investigated in constant-gap, injection-driven, radial Hele-Shaw flows [58–62] and also in centrifugally driven, radial displacements in rotating Hele-Shaw cells with fixed gap thickness [63,64]. However, the analysis of the development of elastic fingering pattern-forming structures in lifting Hele-Shaw cells is still lacking.

The elastic fingering phenomenon was originally observed in an interesting experimental investigation performed by Podgorski *et al.* [58]. Their experiments used two Newtonian fluids of equal viscosities flowing in the usual, constant-gap, injection-driven radial Hele-Shaw setup. The unconventional nature of their system relied on the fact that, when the fluids are brought into contact, a chemical reaction occurs, and the fluid-fluid interface becomes elastic. So the system is composed by two Newtonian fluids, but separated by an elastic contact boundary.

It turns out that the existence of a localized elastic interface in the problem studied in Ref. [58] leads to the emergence of unforeseen dynamical effects, and the rising of peculiar interfacial patterns. It has been observed experimentally [58],

*jme@df.ufpe.br

and later verified theoretically [59,60], that even under zero viscosity difference, the two-fluid interface may become unstable. Moreover, the interfacial patterns obtained in Ref. [58] are completely distinct from the flowerlike morphologies normally detected in conventional viscous fingering experiments, where interfacial elastic effects are absent [24–29]. The elastic fingering patterns at matched viscosity conditions vary from mushroom-shaped fingered structures to quite intricate shapes containing tentaclelike fingers.

More recently, sophisticated numerical simulations [61] and a mode-coupling study [62] have demonstrated that elastic fingering at maximum viscosity contrast conditions (a viscous fluid being displaced by a fluid of negligible viscosity) may result in the appearance of dendritic side-branching and tip-splitting patterns in a Newtonian fluid flow, injection-driven, constant-gap Hele-Shaw system.

Motivated by the fact that the influence of elastic fingering effects on the shape of emerging patterns in lifting Hele-Shaw cells has been overlooked in the literature and stimulated by the suggestive results obtained in Refs. [61,62] regarding the development of dendriticlike elastic fingering structures in Newtonian, fixed-gap Hele-Shaw flows, we carry out our current study. So here we present a weakly nonlinear analysis of the elastic fingering phenomenon in the lifting Hele-Shaw flow arrangement. The main purpose of our work is to offer useful analytical insights into the impact of the elastic interface on the shape of the resulting pattern morphologies, as well as on the habitual finger-competition events that take place during confined lifting flows.

The rest of this paper is outlined as follows. In Sec. II we present the elastic fingering problem in the lifting Hele-Shaw setup and utilize a perturbative weakly nonlinear method to derive a mode-coupling differential equation that describes the time evolution of the interfacial perturbation amplitudes at the early nonlinear regime. In Sec. III we examine how the elastic nature of the fluid-fluid interface influences the intrinsically nonlinear pattern-forming mechanisms of the system. Finally, Sec. IV briefly summarizes our findings and presents chief conclusions and perspectives.

II. GOVERNING EQUATIONS AND THE TIME EVOLUTION OF THE INTERFACIAL DISTURBANCES

The physical system we investigate is constituted by a lifting Hele-Shaw cell of a variable gap width $b(t)$ containing a more viscous fluid of viscosity μ_1, surrounded by a less viscous fluid of viscosity μ_2. The fluids are Newtonian and immiscible, but the interface separating them is elastic. At time $t = 0$ (left panel of Fig. 1), the fluid-fluid interface has a circular shape, presenting radius $R_0 = R(t = 0)$, and initial gap thickness $b_0 = b(t = 0)$. Then, at time $t > 0$ (right panel of Fig. 1), the upper cell plate is lifted along the direction perpendicular to the plates (z axis), and the lower plate is held fixed. The plate separation procedure is executed in such a way that the plates always remain parallel to each other. As the upper plate is moved upwards, the outer fluid 2 is sucked in, and the circular interface retracts. From volume conservation, one can verify that the time-dependent radius of the contracting unperturbed

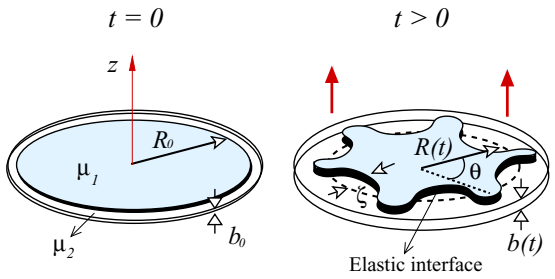

FIG. 1. Representative sketch of the flow in a lifting (time-dependent gap) Hele-Shaw cell presenting an elastic fluid-fluid interface.

interface is given by

$$R(t) = R_0\sqrt{\frac{b_0}{b(t)}}. \tag{1}$$

During the plate-lifting and fluid-sucking process, the viscosity difference between the fluids and the elastic nature of the two-fluid interface give rise to interfacial deformations. In the framework of our weakly nonlinear perturbative model, we describe the deformed fluid-fluid interface as

$$\mathcal{R}(\theta,t) = R(t) + \zeta(\theta,t), \tag{2}$$

where θ represents the azimuthal angle. Here

$$\zeta(\theta,t) = \sum_{n=-\infty}^{+\infty} \zeta_n(t)\exp(in\theta) \tag{3}$$

is the net interface perturbation with Fourier amplitudes $\zeta_n(t)$ and integer wave numbers n. In contrast to purely linear stability analyses (which are linear, i.e., first order, in ζ), our weakly nonlinear approach keeps terms up to the second order in ζ. This allows one to explore analytically the development of key morphological aspects of the elastic fingering interfacial patterns at the onset of nonlinearities.

We follow He *et al.* [59] and consider that the interface separating the fluids behaves as a thin elastic membrane, presenting a curvature-dependent bending rigidity whose value decreases as the local interfacial curvature κ increases:

$$\nu = \nu(\kappa) = \nu_0\left[Ce^{-\lambda^2\kappa^2} + 1 - C\right]. \tag{4}$$

In Eq. (4) ν_0 is the maximum rigidity that expresses the largest resistance to disturbances, and $0 \leqslant C < 1$ is the bending rigidity fraction, which measures the fraction of intramolecular bonds broken through surface deformation. In addition, $\lambda > 0$ denotes a characteristic radius. One can think of the quantity $1/\lambda$ as being a characteristic curvature beyond which $\nu(\kappa)$ has a substantial decrease. Note that the constant bending rigidity limit is reached by setting $C = 0$.

The lifting Hele-Shaw cell system is governed by two gap-averaged equations: Darcy's law [24,46],

$$\mathbf{v}_j = -\frac{b^2(t)}{12\mu_j}\nabla p_j, \tag{5}$$

plus a modified incompressibility condition [1,4,5],

$$\nabla \cdot \mathbf{v}_j = -\frac{\dot{b}(t)}{b(t)}. \tag{6}$$

In Eq. (5) $\mathbf{v}_j = \mathbf{v}_j(r,\theta)$ and $p_j = p_j(r,\theta)$ denote the velocity and pressure in fluids $j = 1,2$, respectively. Moreover, in Eq. (6) $\dot{b}(t) = db(t)/dt$ is the upper plate velocity along the z axis. For lifting flow we have that $\dot{b}(t) > 0$, while for squeeze flow $\dot{b}(t) < 0$. In this paper, we aim attention at the lifting flow case. It is worth noting that the use of Darcy's law (5) implies that the upper plate is neither being lifted fast enough to induce any inertial effects nor being elevated high enough to violate the usual Hele-Shaw assumption of thin fluid layers [$R(t) \gg b(t)$]. As in most experimental and theoretical studies in lifting Hele-Shaw flows [7,12,13,20,33,35,39], we consider a constant lifting speed $\dot{b}(t) = \dot{b} = V$, so that $b(t) = b = b_0 + Vt$. From Eq. (1), one can promptly verify that the velocity of the contracting unperturbed interface $\dot{R}(t) = \dot{R}$ is conveniently related to the upper plate-lifting velocity $\dot{b}(t)$ by the relation $\dot{R} = -(\dot{b}R)/(2b)$.

We proceed by noting that, from the irrotational nature of the flow ($\nabla \times \mathbf{v}_j = 0$), one can define a velocity potential ϕ_j, where $\mathbf{v}_j = -\nabla\phi_j$. By substituting the latter expression into Eq. (6), one can readily verify that ϕ_j obeys the Poisson equation $\nabla^2\phi_j = \dot{b}/b$, having the solution

$$\phi_j(r,\theta) = \sum_{n\neq 0} \phi_{jn}(t)\left(\frac{r}{R}\right)^{(-1)^{(j+1)}|n|} e^{in\theta} + \frac{\dot{b}r^2}{4b}. \tag{7}$$

To get the equation of motion for the interface at $r = \mathcal{R}$, we rewrite Eq. (5) for each of the fluids in terms of the velocity potential. Integrate and then subtract the resulting equations from each other to obtain [27]

$$A\left(\frac{\phi_1+\phi_2}{2}\right)\bigg|_{r=\mathcal{R}} - \left(\frac{\phi_1-\phi_2}{2}\right)\bigg|_{r=\mathcal{R}} = -\frac{b^2(p_1-p_2)|_{r=\mathcal{R}}}{12(\mu_1+\mu_2)}, \tag{8}$$

where $A = (\mu_2-\mu_1)/(\mu_2+\mu_1)$ is the viscosity contrast, a dimensionless viscosity difference between the fluids.

With Eq. (8) at hand, we need to establish the relevant boundary conditions of the problem. First, we consider a generalized Young-Laplace pressure boundary condition that takes into account the contributions coming from the elastic nature of the fluid-fluid interface. Such a pressure boundary condition expresses the pressure jump across the perturbed fluid-fluid interface as [59,60]

$$\begin{aligned}(p_1-p_2)|_{r=\mathcal{R}} = &-\tfrac{1}{2}\nu'''\kappa^2\kappa_s^2 - \nu''\left(3\kappa\kappa_s^2 + \tfrac{1}{2}\kappa^2\kappa_{ss}\right)\\ &- \nu'\left(\tfrac{1}{2}\kappa^4 + 3\kappa_s^2 + 2\kappa\kappa_{ss}\right)\\ &- \nu\left(\tfrac{1}{2}\kappa^3 + \kappa_{ss}\right),\end{aligned} \tag{9}$$

where the curvature-dependent bending rigidity $\nu = \nu(\kappa)$ is given by Eq. (4). In Eq. (9) the primes indicate derivatives with respect to the curvature κ, while the subscripts of κ indicate derivatives with respect to the arc length s. In deriving Eq. (9) we have not taken into account the action of forces associated with moving contact lines at the upper and lower boundaries of the Hele-Shaw cell [60]. As a matter of fact, this is also the case for the other elastic fingering investigations performed by other authors (see, for instance, Refs. [59,61]). The elastic fingering calculations are already sufficiently complicated by neglecting such moving contact line effects, and we are not aware of any existing study that addresses this issue for reactive fingering phenomena in Hele-Shaw geometry. This is beyond the scope of our present work. Moreover, notice that we have also neglected the effect of the transverse interface curvature, which is roughly given by $2/b$. This is justified by the fact that typical lifting velocities are too small, so that the gap thickness b (and consequently, the transverse curvature) does not vary dramatically during the weakly nonlinear stages of the lifting process. Finally, notice that the inclusion of a constant pressure term in Eq. (9) does not affect the motion in our problem, since its gradient is zero [see Eq. (5)].

In addition to the pressure boundary condition (9), we apply the kinematic boundary condition

$$\frac{\partial\mathcal{R}}{\partial t} = \left[\frac{1}{r^2}\frac{\partial r}{\partial\theta}\frac{\partial\phi_j}{\partial\theta} - \frac{\partial\phi_j}{\partial r}\right]_{r=\mathcal{R}}, \tag{10}$$

which states that the normal components of each fluid's velocity are continuous at the interface [24,25]. The tangential components are discontinuous, generating a line of vortices (or, a vortex sheet) at the interface. Even though this tangential velocity condition can be of relevance for determining *stationary* exact solutions for the interface (for example, in rotating Hele-Shaw cells [64]), it is not really useful for the *time-dependent* circumstances of the lifting Hele-Shaw fingering phenomena under study in this work.

At this point, we have all the ingredients needed to find a mode-coupling differential equation that describes the time evolution of the interfacial amplitudes $\zeta_n(t)$. Following traditional steps performed in previous weakly nonlinear studies for Hele-Shaw flows [27,47], first we express ϕ_j [Eq. (7)] in terms of the perturbation amplitudes ζ_n [Eq. (3)] by considering kinematic condition (10). Substituting the resulting relations and the pressure jump condition Eq. (9) into Eq. (8), always keeping terms up to second order in ζ, and Fourier transforming, we obtain the *dimensionless* equation of motion for the perturbation amplitudes (for $n \neq 0$)

$$\dot{\zeta}_n = \Lambda(n)\zeta_n + \sum_{m\neq 0}[F(n,m)\zeta_m\zeta_{n-m} + G(n,m)\dot{\zeta}_m\zeta_{n-m}], \tag{11}$$

where the overdot denotes total time derivative, and

$$\begin{aligned}\Lambda(n) = &-\frac{\mathrm{sgn}(\dot{b})}{2b}(A|n|+1)\\ &+\frac{\Gamma b^{9/2}}{2q^3}|n|(n^2-1)[A_1(C,\eta)(n^2+1)+A_2(C,\eta)],\end{aligned} \tag{12}$$

is the linear growth rate. Notice that the sgn function equals ± 1 according to the sign of its argument. The parameter

$$\Gamma = \frac{\nu_0}{12(\mu_1+\mu_2)R_0^2|\dot{b}|} \tag{13}$$

measures the ratio of elastic to viscous forces, and

$$q = \frac{R_0}{b_0} \tag{14}$$

represents the initial aspect ratio of the system. Moreover,

$$A_1(C,\eta) = Ce^{-\eta}(-4\eta^2 + 10\eta - 2) - 2(1 - C), \tag{15}$$

$$A_2(C,\eta) = Ce^{-\eta}(8\eta^2 - 22\eta + 5) + 5(1 - C), \tag{16}$$

where $\eta = \eta(t) = \lambda^2 b(t)$.

Furthermore, the second-order mode-coupling terms are given by

$$\begin{aligned} F(n,m) = |n|b^{1/2}\Bigg(& -\frac{\mathrm{sgn}(\dot{b})}{2b}\left\{A\left[\mathrm{sgn}(nm) - \frac{1}{2}\right] + \frac{1}{|n|}\right\} \\ & - \frac{\Gamma b^{9/2} C e^{-\eta}}{q^3}[B_1(n,m) + \eta B_2(n,m) \\ & + \eta^2 B_3(n,m) + 2\eta^3 B_4(n,m)] \\ & - \frac{\Gamma b^{9/2}(1 - C)}{q^3} B_1(n,m)\Bigg) \end{aligned} \tag{17}$$

and

$$G(n,m) = b^{1/2}\{A|n|[1 - \mathrm{sgn}(nm)] - 1\}. \tag{18}$$

The expressions for the functions $B_1(n,m)$, $B_2(n,m)$, $B_3(n,m)$, and $B_4(n,m)$ are given in the Appendix.

Expressions (11)–(18) represent the mode-coupling equations of the elastic fingering problem in a lifting Hele-Shaw cell. We nondimensionalized these equations as follows: (i) in-plane lengths are rescaled by R_0; (ii) $b(t)$ is scaled on its initial value b_0; (iii) likewise, time is rescaled by the characteristic time $T = b_0/|\dot{b}(0)|$. We call the reader's attention to the fact that for the rest of this paper we use the dimensionless version of all the equations.

It should be pointed out that the mathematical expressions obtained here for $\Lambda(n)$, Γ, F, and G are similar to the equivalent ones derived for the injection-induced displacement in a constant-gap Hele-Shaw cell [62]. Essentially, in the case of linear growth rate $\Lambda(n)$, the injection rate term shown in Eq. (7) in Ref. [62] is replaced by the plate-lifting velocity term [first term in Eq. (12)]. Similarly, while the parameter Γ defined by Eq. (8) in Ref. [62] involves the injection rate Q in the viscous force contribution, in Eq. (13) above it involves the plate-lifting velocity $|\dot{b}|$. However, this equivalence between Q and $|\dot{b}|$ does not hold at the nonlinear level, and the expression for the function F given by our Eq. (17) differs slightly from the corresponding one shown in Eq. (11) in Ref. [62] due to nonlinear couplings. Finally, notice that the function G given by our Eq. (18) reproduces the one obtained in Ref. [62] [their Eq. (12)] if we use the dimensionless version of Eq. (1), and rewrite $b^{1/2}$ as $1/R$.

Already at the linear level, one can verify that the elastic interface situation for which $C \neq 0$ leads to somewhat unexpected dynamical behaviors. For instance, from the linear growth rate expression [Eq. (12)] one can see that when $C = 0$ [i.e., when $\nu(\kappa) = \nu_0$ is constant], we have $A_1 = -2$ and $A_2 = 5$, meaning that bending forces are stabilizing. However, if $C \neq 0$ the bending rigidity $\nu(\kappa)$ is curvature-dependent [Eq. (4)], and elastic effects may lead to a destabilization of the system. As discussed in Refs. [59,60] for the injection-induced displacement in a constant-gap Hele-Shaw cell, such a destabilization process can occur even if the system is not viscosity driven. In the lifting flow case, this signifies that the system could become linearly unstable, even if the viscosity contrast is zero or positive ($0 \leqslant A \leqslant 1$).

Despite the appealing nature of the linear destabilizing mechanism described above, once it has been extensively studied in Refs. [59,60], here we concentrate on the impact of the elastic effects on the early nonlinear dynamics of the system. More specifically, we investigate how the curvature-dependent elastic effects influence the weakly nonlinear shape of the patterns formed under confined lifting flow. Throughout this work, we focus on the important maximum viscosity contrast situation $A = -1$, which is the most explored in both real experiments and numerical simulations of the lifting Hele-Shaw cell problem [5,7,12,13,15,20,33,35,39].

We emphasize that the values we take for all other parameters considered in this study are consistent with typical physical quantities used in these experimental and numerical investigations. The specific values of the various physical parameters we used in our calculations are taken from Refs. [5,7,12,13,15,20,33,35,39]: $\dot{b} = \mathcal{O}(10^{-6})$ m/s, $b_0 = \mathcal{O}(10^{-4})$ m, $R_0 = \mathcal{O}(10^{-2})$ m, $\mu_1 = \mathcal{O}(10^2)$ Pa s, and $\mu_2 = 0$. Under such characteristic conditions we take the initial aspect ratio as $200 \leqslant q \leqslant 300$. It is worth mentioning that for this set of input parameters the Reynolds number of the system, $\mathrm{Re} = \rho|\dot{R}|/12\mu_1 = \mathcal{O}(10^{-4})$, where $\rho_1 = \mathcal{O}(10^3)\mathrm{kg/m^3}$ ($\rho_2 = 0$) is the density of the inner (outer) fluid, is very small so that inertial effects can be safely neglected. In addition, the parameters related to the elastic fingering phenomenon are taken from Refs. [58,59,61] and are given as follows: $\nu_0 = \mathcal{O}(10^{-8})$ kg m^2/s^2, $0 \leqslant C \leqslant 0.5$, $0.10 \leqslant \Gamma \leqslant 0.15$, and $0.50 \leqslant \lambda \leqslant 0.85$.

Before we advance to the next section, it is worth pointing out that when $C = 0$, the exponential term in Eq. (4) vanishes, and we obtain a constant bending rigidity situation in which $\nu = \nu(\kappa) = \nu_0$. This leads to a much simpler pressure jump boundary condition expression [see Eq. (9)], involving only a constant (ν_0) multiplying derivatives of the interfacial curvature κ. This $C = 0$ expression for the pressure jump condition resembles the expression usually obtained in traditional Hele-Shaw cell problems where elastic effects are not considered [24]. In this traditional case, the pressure jump is simply represented by the product of a constant (surface tension) by κ. In this sense, one could expect that in the $C = 0$ limit the constant bending rigidity ν_0 would act similarly to surface tension, having a stabilizing role. On the other hand, when $C \neq 0$ and $\nu(\kappa)$ is legitimately curvature-dependent, the bending rigidity could also destabilize the interface, and much more interesting effects may arise.

III. WEAKLY NONLINEAR BEHAVIOR OF THE ELASTIC FINGERING PATTERNS

In this section, we use the set of Eqs. (11)–(18) and employ a weakly nonlinear theory to elucidate key aspects related to finger-shape behavior and finger-competition dynamics in the lifting Hele-Shaw flow problem, when the fluid-fluid interface is elastic. In order to simplify our discussion, we conveniently

rewrite the net perturbation [Eq. (3)] in terms of cosine and sine modes,

$$\zeta(\theta,t) = \zeta_0 + \sum_{n=1}^{\infty}[a_n(t)\cos(n\theta) + b_n(t)\sin(n\theta)], \qquad (19)$$

where $a_n = \zeta_n + \zeta_{-n}$ and $b_n = i(\zeta_n - \zeta_{-n})$ are real valued. In the Fourier expansion (19), we include the $n = 0$ mode to maintain the area of the perturbed shape independent of the perturbation ζ. Mass conservation imposes that the zeroth mode is written in terms of the other modes as

$$\zeta_0 = -\frac{1}{4R}\sum_{n=1}^{\infty}\left[a_n^2(t) + b_n^2(t)\right]. \qquad (20)$$

Without loss of generality, we may choose the phase of the fundamental mode so that $a_n > 0$ and $b_n = 0$.

It is well known [24] that the main pattern-forming mechanisms of the viscous fingering process in conventional, injection-driven Hele-Shaw flows (in the absence of interfacial elastic effects) can be identified as spreading, splitting, and competition. In late 1990s, it was shown that these basic mechanisms could be consistently mimicked by considering the weakly nonlinear coupling of just a few participating Fourier modes [27,47]: (i) The characteristic shape of the fingers (finger widening and narrowing) could be given by the interplay between a fundamental mode n and its first-harmonic cosine mode $2n$, while (ii) finger-competition events (related to finger-length variability) could be described by the interaction of a fundamental mode n and its sine and cosine subharmonic modes $n/2$.

Later on, it has also been demonstrated that the mechanism of side-branching formation for the flow of non-Newtonian (shear-thinning) [50–57] fluids in the injection-induced, radial Hele-Shaw problem (still neglecting interfacial elastic effects) would require the presence of mode $3n$ [55,57]. In this way, the detected dendriticlike growth could be reproduced by considering the nonlinear coupling between a fundamental mode n and its harmonics $2n$ and $3n$. Similar to what we recently did in Ref. [62] for the study of elastic fingering formation in the injection-driven problem under constant-gap circumstances, we use the mode-coupling picture introduced in [27,47,55] to probe the basic morphology of the elastic fingering patterns generated in a lifting Hele-Shaw cell. For a detailed discussion about the mode-coupling strategy, its description and proposed interpretation of the typical pattern-forming mechanisms occurring in Hele-Shaw flows, we refer the readers to Refs. [27,47,55,57].

A. The shape of the fingers: Occurrence of tip splitting and side branching

We begin our discussion by examining the finger-shape behavior at the weakly nonlinear level. As commented earlier, finger-tip-narrowing, -tip-broadening, and -tip-splitting phenomena can be described by considering the influence of a fundamental mode n on the growth of its harmonic $2n$. For lifting flow, it can be shown [14,27] that an enhanced tendency of the inward-moving fingers of the outer fluid to get wider (narrower) occurs when $a_{2n} > 0$ ($a_{2n} < 0$). So, a positive growth for the cosine amplitude of the first harmonic mode $2n$ would mean tendency toward finger-tip-splitting formation of the invading fingers of the outer fluid. Likewise, as proposed in Refs. [55,57], if the harmonic cosine mode amplitude a_{3n} is positive and sufficiently large, it can produce interfacial lobes branching out sidewards, leading to side-branching formation.

Therefore, to properly evaluate the resulting shape of the fingers during lifting Hele-Shaw flows with an elastic interface, we consider the simultaneous action of the three morphologically relevant modes n, $2n$, and $3n$, and rewrite the mode-coupling equation (11) in terms of the cosine amplitudes to get

$$\dot{a}_n = \lambda(n)a_n + \tfrac{1}{2}\{[T(n,-n) + T(n,2n)]a_n a_{2n} + [T(n,3n) + T(n,-2n)]a_{2n}a_{3n}\}, \qquad (21)$$

$$\dot{a}_{2n} = \lambda(2n)a_{2n} + \tfrac{1}{2}\{T(2n,n)a_n^2 + [T(2n,-n) + T(2n,3n)]a_n a_{3n}\}, \qquad (22)$$

and

$$\dot{a}_{3n} = \lambda(3n)a_{3n} + \tfrac{1}{2}[T(3n,n) + T(3n,2n)]a_n a_{2n}, \qquad (23)$$

where

$$T(n,m) = F(n,m) + \lambda(m)G(n,m). \qquad (24)$$

Note that, for consistent second-order expressions, on the right-hand side of Eqs. (21)–(23) we replaced time derivative terms like $\dot{a}_n$ with $\lambda(n)a_n$. The time evolution of the amplitudes $a_n(t)$, $a_{2n}(t)$, and $a_{3n}(t)$ can be obtained by numerically solving the coupled nonlinear differential equations (21)–(23).

It should be stressed that the task of searching for possible pattern-forming morphologies in the elastic fingering problem through a weakly nonlinear strategy is not exactly trivial. First, notice that we have to deal with a multidimensional parameter space, containing four relevant controlling quantities, namely, C, λ, Γ, and q. On top of that, to guarantee the generality of the results, we have to explore and test various possible sets of initial conditions for the perturbation amplitudes. Finally, while varying physical parameters and initial conditions, we also have to make sure that our second-order mode-coupling theory remains valid for the whole range of time intervals considered during the quest for attainable patterns. Despite the relative simplicity of our theoretical approach, we urge the reader to keep in mind that considerable effort and caution are necessary in order to properly address, and surpass, all these intrinsic difficulties. However, once this is done, one can extract valuable physical information about the fundamental architecture of the underlying pattern-forming structures already at early nonlinear stages of the dynamics.

In Figs. 2 and 3 we illustrate the typical pattern morphologies that may arise in lifting flows with Newtonian fluids if the presence of an elastic two-fluid interface is taken into consideration. In the left panels of these figures, we plot the time evolution of the contracting fluid-fluid interface for three increasing values of the bending rigidity fraction C. This is done by utilizing Eqs. (19) and (20) and considering the nonlinear interaction of the three relevant cosine modes, n, $2n$, and $3n$, as prescribed by Eqs. (21)–(23). In order to facilitate the visualization of the morphological details of the resulting

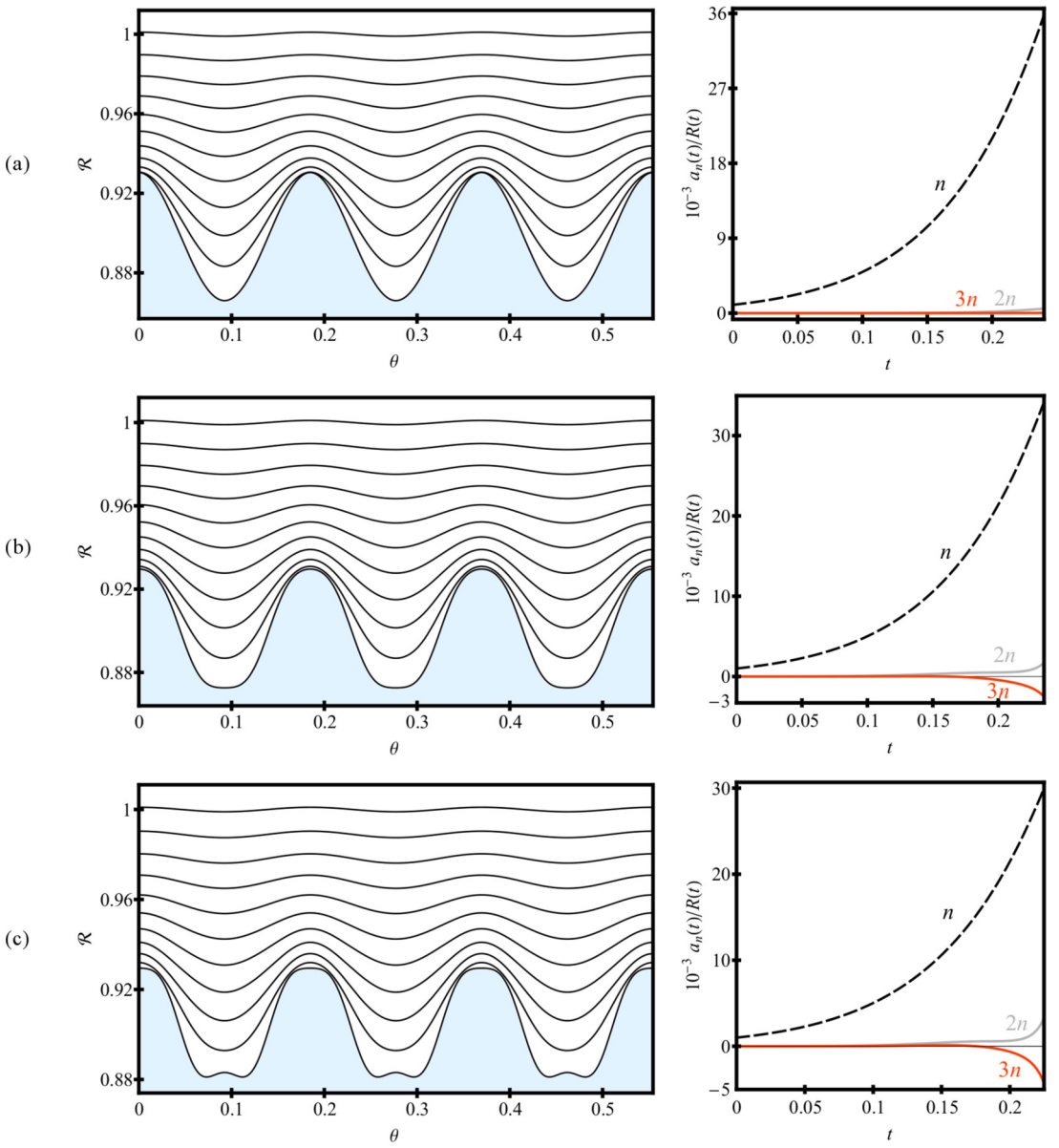

FIG. 2. Time evolution of the fluid-fluid interface position $\mathcal{R}$ as a function of the polar angle θ (left panels), illustrating the representative elastic fingering patterns that may emerge during lifting Hele-Shaw flows. The corresponding time evolution of the rescaled cosine amplitudes $a_n(t)/R(t)$ for modes n, $2n$, and $3n$, where $n = 34$, is depicted in the right panels. The values of the bending rigidity fraction parameter are (a) $C = 0$, (b) $C = 0.35$, and (c) $C = 0.45$. In addition, $\Gamma = 0.1$, $q = 300$, and $\lambda = 0.85$. The final times used are (a) $\tau = 0.240$, (b) $\tau = 0.235$, and (c) $\tau = 0.225$. Note that the polar angle θ is given in radians.

fingering structures, for each time t, we plot the interface position $\mathcal{R}$ as a function of the polar angle θ in such a way that only a few fingers are shown. This is done because the plot of the entire two-fluid interface for $0 \leqslant \theta \leqslant 2\pi$ involves a larger number of relatively small penetrating fingers, for which the identification of the interfacial features is much more difficult. Notice that, as represented in the left panels of Figs. 2 and 3, the direction of the flow is from top to bottom (direction of decreasing R).

In the plots presented in Figs. 2 and 3, we take the initial conditions $a_n(0) = 10^{-3}$, and $a_{2n}(0) = a_{3n}(0) = 0$ so that modes $2n$ and $3n$ are both initially absent. In addition, $\Gamma = 0.1$ and $q = 300$. The time varies in the interval $0 \leqslant t \leqslant \tau$, where τ is the time at which successive interfaces are about to cross one another. Since this crossing is not detected in experiments and fully nonlinear simulations in lifting Hele-Shaw flows [13,20], we adopt the largest time before crossing as the upper bound time ($t = \tau$) for the validity of our theoretical description. Note that the values of τ and $b(t = \tau)$ we use throughout this work are consistent with the thin-layer approximation mentioned in Sec. II right after presenting Eqs. (5) and (6). This approximation holds because the typical lifting velocities are very small, so that b does not vary much for the lifting process that occurs during the weakly nonlinear regime considered in our current study. Finally, in the right panels of Figs. 2 and 3, for each value of C, we depict we the time evolution of the rescaled

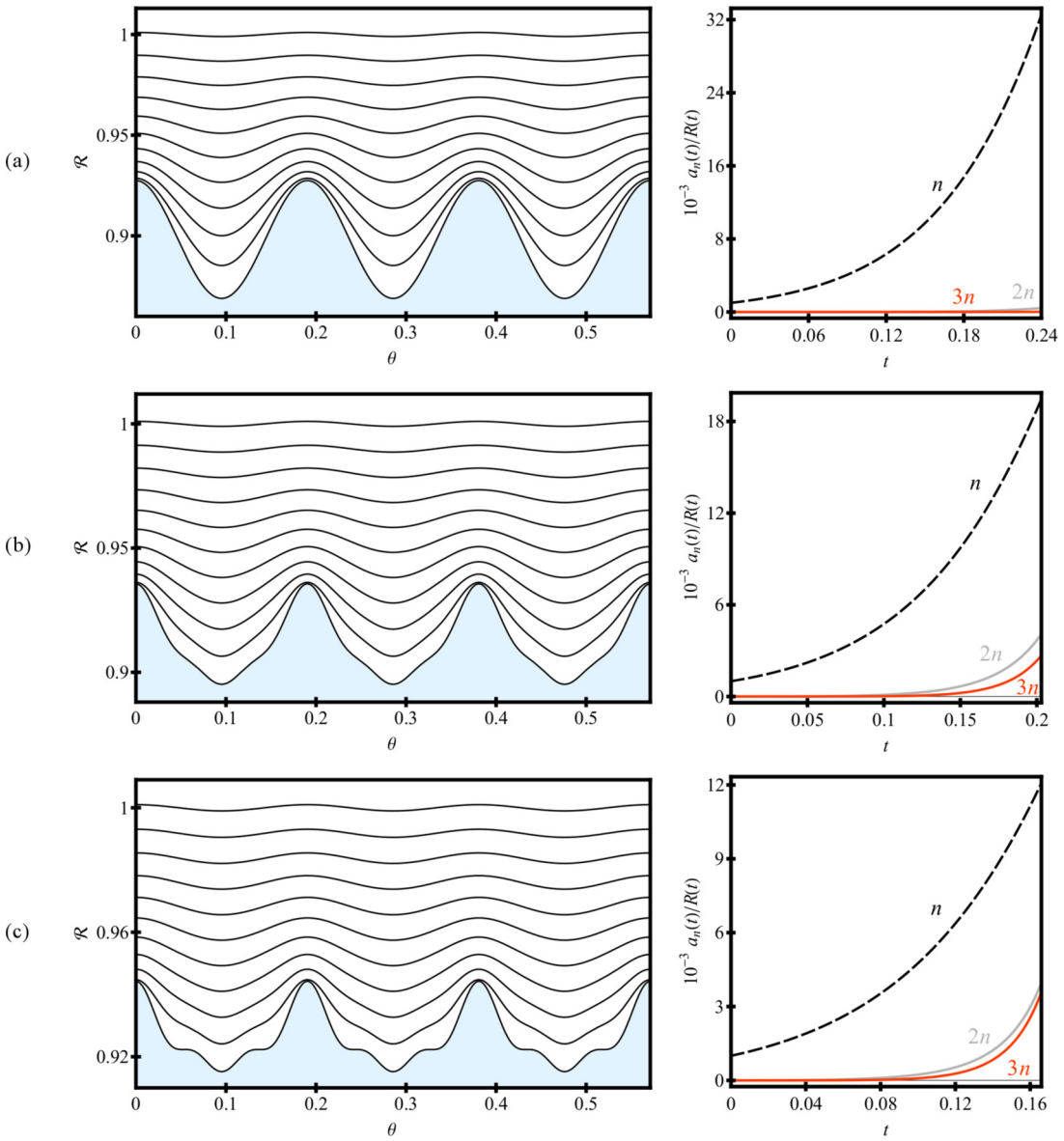

FIG. 3. Time evolution of the fluid-fluid interface position $\mathcal{R}$ as a function of the polar angle θ (left panels), illustrating the typical elastic fingering patterns that may arise during lifting Hele-Shaw flows. The corresponding time evolution of the rescaled cosine amplitudes $a_n(t)/R(t)$ for modes n, $2n$, and $3n$, where $n = 33$, is depicted in the right panels. The values of the bending rigidity fraction parameter are (a) $C = 0$, (b) $C = 0.125$, and (c) $C = 0.25$. In addition, $\Gamma = 0.1$, $q = 300$, and $\lambda = 0.7$. The final times used are (a) $\tau = 0.240$, (b) $\tau = 0.203$, and (c) $\tau = 0.166$. The polar angle θ is given in radians.

cosine amplitudes $a_n(t)/R(t)$ for the three participating modes.

Before we continue, it is important to discuss the reason for the choice of the fundamental mode n plotted in Figs. 2, 3, and 4. First of all, it should be pointed out that, under lifting Hele-Shaw circumstances, the number of fingers varies quite dramatically as the controlling parameters of the system (λ, Γ, q, and C) are changed. On the other hand, in order to search for the possible different pattern morphologies under lifting flow, one has to sweep different regions of the parameter space. To do this, we varied the possible values of the controlling parameters by requiring that the relevant participating Fourier modes would remain linearly unstable during the whole lifting process. This would allow one to observe growth of all modes involved. In other words, for the tip-splitting and side-branching cases, we require that modes n, $2n$, and $3n$ are linearly unstable up until time τ. This has been done by imposing that the largest Fourier mode among n, $2n$, and $3n$ is the critical mode at $t = \tau$. This corresponds to setting $\Lambda(3n) = 0$ at $t = \tau$, ensuring that $3n$ is a critical mode at the final time, so that modes n, $2n$, and $3n$ always remain inside of the band of unstable modes during the entire lifting procedure. Something similar has also been done in the finger-competition case to be investigated in Sec. III B, in which the relevant participating modes are n and $n/2$. In this case, we equivalently imposed the condition $\Lambda(n) = 0$ at $t = \tau$. In conclusion, for a given set of parameters λ, Γ, q, and C, the number of fingers is set by imposing the condition

$\Lambda(3n) = 0$ at $t = \tau$ for the tip-splitting and side-branching cases (Figs. 2 and 3) and by the condition $\Lambda(n) = 0$ at $t = \tau$ for the finger-competition situation (Fig. 4).

Our search for the possible shapes assumed by the fingers as the upper Hele-Shaw cell plate is lifted begins with the inspection of Fig. 2. In this situation, we take $\lambda = 0.85$ and consider the following values for the bending rigidity fraction parameter: (a) $C = 0$, (b) $C = 0.35$, and (c) $C = 0.45$. First, we analyze the case in which interfacial elastic effects are independent of the interfacial curvature [Fig. 2(a)]. Under such circumstances, nothing really unexpected happens, and the morphology of the fingers is basically defined by the growth of the fundamental mode n, which reaches significantly larger amplitudes than the modes $2n$ and $3n$. This is clearly illustrated by the growth of amplitudes represented in the right panel of Fig. 2(a). Therefore, when $C = 0$, the amplitudes a_{2n} and a_{3n} are very small, and there is no sign of either tip splitting or side branching.

An evidently different behavior is revealed in Fig. 2(b), when the elastic effects depend on the curvature of the fluid-fluid interface. Even though, for initial times, the interface evolution in Fig. 2(b) is not that distinct from the one shown in Fig. 2(a), as time advances one verifies that the tips of the invading fingers of the outer fluid get wider and at late times become progressively blunt, revealing the occurrence of a finger-tip-flattening process. Within the scope of our mode-coupling description, the reason for this morphological behavior is that, nonlinear elastic effects favor the growth of the first harmonic mode $2n$, with a positive amplitude a_{2n} [see the right panel of Fig. 2(b)]. Consistent with comments earlier in this section, this is precisely the phase of mode $2n$ that leads to finger-tip broadening, and then to finger-tip flattening. On the other hand, the mode $3n$ presents a negative phase, so that side-branching formation is not favored [55,57]. In Fig. 2(b) the fact that $C \neq 0$ is indicative that the finger-tip-flattening behavior is activated by the curvature-dependent nature of the bending rigidity.

An even more emblematic dynamic response is observed in Fig. 2(c), where C is nonzero and larger than the corresponding value used in Fig. 2(b). By examining Fig. 2(c), one can see that the invading fingers are not only broadened as time progresses, but their tips ultimately split. In fact, the enhanced growth of mode $2n$ for this situation can be easily visualized in the right panel of Fig. 2(c). Once again, we see that $a_{3n} < 0$, and no side branching emerges. More physically speaking, the development of finger-tip splitting in Fig. 2(c) is provoked by an increase in the bending rigidity $\nu(\kappa)$ [Eq. (4)] at the tip of the finger. This increase in $\nu(\kappa)$ is sufficient to suppress local curvature growth, thus favoring the finger to split along regions of reduced rigidity, as determined by the favored growth of mode $2n$.

Some of the observations made during the analysis of Fig. 2 are somewhat surprising, in particular, the one related to the occurrence of finger tip-splitting, which is not at all common for lifting flow with Newtonian fluids. As discussed in Sec. I, tip splitting in Newtonian lifting flows occurs only at extreme conditions [48] (for example, at quite high lifting velocities), which is *not* the case here. As already pointed out, the dimensionless parameters we use are absolutely consistent with typical, real experimental conditions [12,13,20,33,39] and have not been exaggerated. So here, although the fluids are Newtonian and the parameter values unexceptional, finger-tip splitting can still be observed. In fact, the key element in our system is the elastic nature of the fluid-fluid interface: Curvature-dependent elastic effects localized at the interface are the ones responsible for inducing finger-tip broadening, finger-tip flattening, as well as finger-tip splitting.

As we continue in our pursuit of other possible pattern-forming behaviors, we now examine Fig. 3. Similar to what we did in Fig. 2, Fig. 3 plots the evolution of the fluid-fluid interfaces in the left panels and the corresponding time advancement of the rescaled perturbation amplitudes $a_n(t)/R(t)$ in the right panels. Figure 3 considers the same initial conditions utilized in Fig. 2, and other than taking different values of C, the most basic difference regarding physical parameters is the fact that we set a distinct value for the characteristic radius, so that now $\lambda = 0.7$. In essence, to find something other than tip splitting, we wanted to keep everything as close as possible to the physical circumstances utilized in Fig. 2 and systematically varied λ up to a point at which some other interfacial behavior could be unveiled.

Figure 3(a) addresses the situation in which the effects of the elastic interface are curvature independent (i.e., $C = 0$). As in the case of Fig. 2(a), nothing really peculiar is shown in Fig. 3(a), and reasonably unstructured pointy fingers are produced. The shape of the interface is mostly defined by the fundamental mode n, which grows considerably larger than modes $2n$ and $3n$, as shown in the right panel of Fig. 3(a). However, something notably different is observed in Fig. 3(b), when the bending rigidity fraction is nonzero ($C = 0.125$): As the interface evolves, one notices that the morphology of penetrating inward-moving fingers of the outer fluid begin to change, becoming sharper at their tips and wider at their sides. By observing the right panel of Fig. 3(b), one can see that this suggestive event is due to the favored growth of both harmonic modes $2n$ and $3n$, which now have sizable positive amplitudes. Note that now $a_{3n} > 0$ and side branching could occur.

Then, by inspecting Fig. 3(c), which takes an even larger value of C (now $C = 0.25$), one encounters something rather interesting, namely the rising of broadened, threefold-shaped fingering structures, showing interfacial lobes that branch out sideways. This produces the formation of side-branching patterns in our elastic fingering system. Such a curious pattern-forming behavior can be justified by resorting to our mode-coupling approach: From the right panel of Fig. 3(c) one can readily see that this is induced by the enhanced growth of mode $3n$ (with the proper positive phase), that in conjunction with the growth of mode $2n$, results in side-branched finger shapes. It is important to underline that here, similar to what was discussed in Fig. 2 regarding tip splitting, the side-branching phenomenon identified in Fig. 3 is *not* due to the non-Newtonian nature of the fluids (after all, the fluids are Newtonian), but driven by the curvature-dependent elastic effects that arise at the interface separating them. The elastically induced side-branching phenomenon depicted in Fig. 3(c) can be explained on more physical grounds by the dynamical increase in the bending rigidity $\nu(\kappa)$ along the directions of increased local curvature, as defined by the stimulated growth of modes $3n$ and $2n$.

As we close this section, it should be stressed that we have searched for other types of patterns within and beyond the range of parameters (C, λ, Γ, q) and initial conditions considered in Figs. 2 and 3, but have not found any other significantly distinct type of patterned morphologies than the ones already presented in this work. Therefore, at least within the scope of our weakly nonlinear theory, one can say that the two basic morphological mechanisms for elastic fingering formation in lifting confined flows are indeed tip splitting and side branching.

B. Impact of elastic effects on finger competition

In addition to the characteristic shape of the fingers discussed in Sec. III A, as already commented in Sec. I, another salient aspect verified during lifting Hele-Shaw flows is the phenomenon of finger competition. Regardless, the specific nature of the fluids (Newtonian or non-Newtonian), numerical simulations, and experiments [5,10,12,13,15–17,19,20,33] consistently reveal a situation in which slow penetrating fingers of the outer, less viscous fluid are outrun by surrounding invading fingers that move faster. So, manifestly, there exists a competition (i.e., a finger-length variability) among the fingers of the invading less viscous fluid, which advance towards the center of the cell. Taking into consideration the importance of the finger-competition dynamics to lifting Hele-Shaw flows in general, in this section we examine the effect of the elastic fluid-fluid interface on finger-competition events.

We follow Ref. [27], and consider finger-length variability as a measure of the competition among fingers. Within our mode-coupling approach, the finger-competition mechanism is described by the influence of a fundamental mode n, assuming n is even, on the growth of its subharmonic mode $n/2$. By utilizing Eqs. (11)–(18), the equations of motion for the subharmonic mode can be written as

$$\dot{a}_{n/2} = \{\lambda(n/2) + \mathcal{C}(n,t)a_n\}a_{n/2}, \tag{25}$$

$$\dot{b}_{n/2} = \{\lambda(n/2) - \mathcal{C}(n,t)a_n\}b_{n/2}, \tag{26}$$

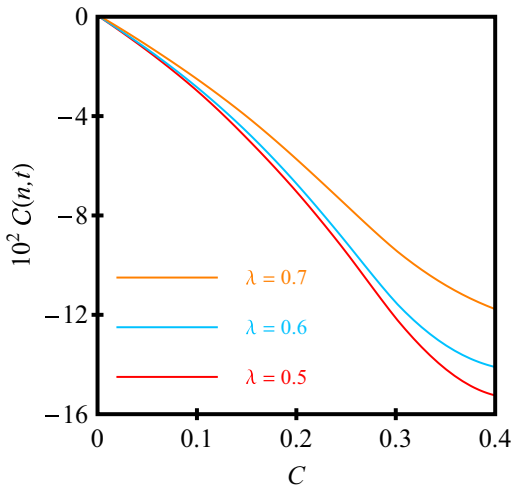

FIG. 4. Behavior of the finger-competition function $\mathcal{C}(n,t)$ as the bending rigidity fraction C is varied for three values of the characteristic radius λ.

where

$$\mathcal{C}(n,t) = \left\{\frac{1}{2}\left[F\left(-\frac{n}{2},\frac{n}{2}\right) + \lambda(n/2)G\left(\frac{n}{2},-\frac{n}{2}\right)\right] + \frac{1}{2}\left[F\left(\frac{n}{2},n\right) + \lambda(n)G\left(\frac{n}{2},n\right)\right]\right\} \tag{27}$$

is the finger-competition function. As we have done in Eqs. (21)–(23), for consistent second-order expressions, on the right-hand side of Eqs. (25) and (26) we replaced time-derivative terms like $\dot{a}_n$ and $\dot{b}_n$ with $\lambda(n)a_n$ and $\lambda(n)b_n$, respectively.

Now we briefly discuss how one can use Eqs. (25) and (26) and the function $\mathcal{C}(n,t)$ to get valuable information about the finger-competition behavior in our problem. By inspecting Eqs. (25) and (26) and recalling that $a_n > 0$, we verify that a negative $\mathcal{C}(n,t)$ increases the growth of the sine subharmonic $b_{n/2}$, while inhibiting growth of its cosine subharmonic $a_{n/2}$. The result is an increased variability among the lengths of fingers of the outer fluid 2 penetrating into the inner fluid 1. This effect describes the competition of inward-moving fingers of fluid 2. Notice that the magnitude of the function $\mathcal{C}(n,t)$ as given by Eq. (27) measures the strength of the competition; i.e., increasingly larger absolute values of $\mathcal{C}(n,t)$ lead to enhanced finger competition. Remember that what is observed in experiments and numerical simulations of the lifting flow problem (in the absence of elastic effects) [5,7,12,13,15,20,33,35,39] is, in fact, the competition of the inward-moving fingers of the outer fluid. These observations are consistent with a negative finger-competition function.

Of course, reversing the sign of $\mathcal{C}(n,t)$ would exactly reverse conclusions we reached in the previous paragraph, such that modes $a_{n/2}$ would be favored over modes $b_{n/2}$. In other words, a positive $\mathcal{C}(n,t)$ would indicate increased competition among the outward pointing fingers of fluid 1, something that is not observed in Refs. [5,7,12,13,15,20,33,35,39].

To illustrate a typical influence of the interfacial elastic effects on the finger-competition behavior at second order, in Fig. 4 we plot $\mathcal{C}(n,t)$ as a function of the bending rigidity fraction C for three values of the characteristic radius $\lambda = 0.5$, 0.6, and 0.7. As discussed earlier, to observe growth of modes $n/2$ and n, we carry out our finger-competition analysis by considering that $\Lambda(n) = 0$ at $t = \tau$. Here we consider that $n = 62$ for $\lambda = 0.5$ and $\lambda = 0.6$ and $n = 64$ for $\lambda = 0.7$. The initial amplitudes are taken as $a_{n/2}(0) = b_{n/2}(0) = a_n(0) = 10^{-3}$. In addition, we set $\Gamma = 0.15$ and $q = 200$.

From Fig. 4, first we notice that the finger-competition function $\mathcal{C}(n,t)$ assumes only negative values for $C > 0$. This indicates favored finger competition among the inward-pointing fingers of the less viscous, penetrating fluid. This initial verification is somewhat reassuring, in the sense that it is in line with what is usually observed in conventional lifting Hele-Shaw flows. Another evident behavior is the fact that, regardless the value of λ, the function $\mathcal{C}(n,t)$ becomes increasingly more negative if C is increased. This means that, for a given value of λ, finger competition tends to become more intense for larger C. Finally, it is also apparent that the finger competition depends on the value of λ, where for a fixed C, larger values of λ tend to decrease competition among inward-moving fingers. This can be explained as follows. Since

λ is a characteristic radius beyond which the bending rigidity has a substantial decrease [see Eq. (4)], for such higher values of λ one has a significant decay of the elastic effects already at the beginning of the lifting process. This leads to a less intense, elastic-driven competition effects. All these findings demonstrate that the finger-competition scenario in confined lifting flows is, in fact, sensitive to changes in the basic elastic properties of the two-fluid interface and that it can be regulated by manipulating C and λ.

IV. CONCLUDING REMARKS

A large body of experimental and theoretical (both analytical and numerical) research on the lifting Hele-Shaw problem with Newtonian fluids shows that the resulting fluid-fluid interfacial patterns involve the development of smooth penetrating fingers that compete among themselves. However, if the lifted fluids are non-Newtonian, a markedly different set of patterns arise: Although competition among inward-moving fingers is still present, the shapes of these fingers are much more irregular, revealing the occurrence of finger-tip-splitting and side-branching phenomena.

In this work, we have investigated a particular variant of the traditional lifting Hele-Shaw problem that, in spite of containing just Newtonian fluids, may still lead to the formation of tip splitting and side branching. This somewhat unexpected pattern-forming behavior emerges due to the presence of a fluid-fluid interface that acts like an elastic membrane, presenting a curvature-dependent bending rigidity. By employing a perturbative mode-coupling approach, we have been able to predict the appearance of such suggestive elastic fingering structures (displaying split or side-branched fingers), already at the lowest nonlinear level of the dynamics. The influence of the elastic interface on the competition among penetrating fingers has also been examined, indicating that the competition events are indeed sensitive to changes in the characteristic radius λ, and in the bending rigidity fraction C. More precisely, we have found that elastic-induced finger-competition effects tend to increase for larger values of C, and smaller values of λ.

The theoretical predictions presented in this work have not yet been ratified by fully nonlinear numerical simulations and laboratory experiments. Despite the possibly challenging nature of such studies, they constitute two possible avenues within the scope of future work on the topic of elastic fingering pattern formation in lifting confined flows. Incidentally, during the course of our present research, it has been brought to our attention that Professor Shuwang Li and collaborators are working on a numerical investigation of elastic fingering in the lifting Hele-Shaw cell arrangement. Their study explores fully nonlinear aspects of the problem, utilizing the powerful numerical scheme they have recently reported in Ref. [61], as well as the numerical techniques presented in Refs. [29,65]. Hopefully, these and other investigators will have the opportunity to check some of our findings.

Possible extensions of this work could address the current limitations of our theoretical model: for instance, (i) inclusion of forces associated with the moving contact line at upper and lower cell boundaries; (ii) consideration of Laplace pressure effects related to the interfacial curvature along the transverse direction to the cell plates; (iii) formation of new elastic interfaces as b is increased; (iv) addition of inertial effects and generalization to higher Reynolds number situations; and (v) a more systematic exploration of the parameter space.

ACKNOWLEDGMENT

J.A.M. thanks CNPq (Brazilian Research Council) for financial support under Grant No. 304821/2015-2.

APPENDIX: FUNCTIONS APPEARING IN THE MODE-COUPLING TERM $F(n,m)$

This appendix presents the expressions for the functions $B_1(n,m)$, $B_2(n,m)$, $B_3(n,m)$, and $B_4(n,m)$, which appear in Eq. (17) of the text

$$\begin{aligned} B_1(n,m) = &-3 + \frac{15}{4}m(n-m) + 10(n-m)^2 \\ &- \frac{9}{2}m^2(n-m)^2 - 6m(n-m)^3 \\ &- 4(n-m)^4, \end{aligned} \tag{A1}$$

$$\begin{aligned} B_2(n,m) = &\frac{39}{2} - 30m(n-m) - 71(n-m)^2 \\ &+ \frac{81}{2}m^2(n-m)^2 + 54m(n-m)^3 \\ &+ 32(n-m)^4 - 12m^2(n-m)^4 \\ &- 12m^3(n-m)^3, \end{aligned} \tag{A2}$$

$$\begin{aligned} B_3(n,m) = &-14 + 25m(n-m) + 54(n-m)^2 \\ &- 36m^2(n-m)^2 - 48m(n-m)^3 \\ &- 26(n-m)^4 + 18m^2(n-m)^4 \\ &+ 18m^3(n-m)^3, \end{aligned} \tag{A3}$$

and

$$\begin{aligned} B_4(n,m) = &1 - 2m(n-m) - 4(n-m)^2 \\ &+ 3m^2(n-m)^2 + 4m(n-m)^3 \\ &+ 2(n-m)^4 - 2m^2(n-m)^4 \\ &- 2m^3(n-m)^3. \end{aligned} \tag{A4}$$

[1] E. Ben-Jacob, R. Godbey, N. D. Goldenfeld, J. Koplik, H. Levine, T. Mueller, and L. M. Sander, Phys. Rev. Lett. **55**, 1315 (1985).

[2] H. La Roche, J. F. Fernández, M. Octavio, A. G. Loeser, and C. J. Lobb, Phys. Rev. A **44**, R6185 (1991).

[3] A. A. Sonin and R. Bartolino, Nuovo Cimento D **15**, 1 (1993).

[4] S.-Z. Zhang, E. Louis, O. Pla, and F. Guinea, Eur. Phys. J. B **1**, 123 (1998).

[5] M. J. Shelley, F.-R. Tian, and K. Wlodarski, Nonlinearity **10**, 1471 (1997).

[6] J. Bohr, S. Brunak, and T. Nørretranders, Europhys. Lett. **25**, 245 (1994).
[7] S. Roy and S. Tarafdar, Phys. Rev. E **54**, 6495 (1996).
[8] S. K. Thamida, P. V. Takhistov, and H.-C. Chang, Phys. Fluids **13**, 2190 (2001).
[9] S. Sinha, S. K. Kabiraj, T. Dutta, and S. Tarafdar, Eur. Phys. J. B **36**, 297 (2003).
[10] S. K. Kabiraj and S. Tarafdar, Phys. A (Amsterdam, Neth.) **328**, 305 (2003).
[11] C.-Y. Chen, C.-H. Chen, and J. A. Miranda, Phys. Rev. E **71**, 056304 (2005).
[12] M. Ben Amar and D. Bonn, Phys. D (Amsterdam, Neth.) **209**, 1 (2005).
[13] A. Lindner, D. Derks, and M. J. Shelley, Phys. Fluids **17**, 072107 (2005).
[14] R. M. Oliveira and J. A. Miranda, Phys. Rev. E **73**, 036309 (2006).
[15] A. Tatulchenkov and A. Cebers, Phys. Fluids **20**, 054101 (2008).
[16] J. Nase, A. Lindner, and C. Creton, Phys. Rev. Lett. **101**, 074503 (2008).
[17] S. Sinha, T. Dutta, and S. Tarafdar, Eur. Phys. J. E **25**, 267 (2008).
[18] S. Tarafdar, S. Sinha, S. Nag, and T. Dutta, Phys. Rev. E **80**, 026315 (2009).
[19] S. Tarafdar, S. Nag, T. Dutta, and S. Sinha, Pramana **73**, 743 (2009).
[20] J. Nase, D. Derks, and A. Lindner, Phys. Fluids **23**, 123101 (2011).
[21] E. O. Dias and J. A. Miranda, Phys. Rev. E **88**, 043002 (2013).
[22] R. E. Goldstein, H. E. Huppert, H. K. Moffatt, and A. I. Pesci, J. Fluid Mech. **753**, R1 (2014).
[23] Z. Zheng, H. Kim, and H. A. Stone, Phys. Rev. Lett. **115**, 174501 (2015).
[24] G. M. Homsy, Annu. Rev. Fluid Mech. **19**, 271 (1987); K. V. McCloud and J. V. Maher, Phys. Rep. **260**, 139 (1995).
[25] L. Paterson, J. Fluid Mech. **113**, 513 (1981).
[26] J. D. Chen, J. Fluid Mech. **201**, 223 (1989).
[27] J. A. Miranda and M. Widom, Phys. D (Amsterdam, Neth.) **120**, 315 (1998).
[28] J. Mathiesen, I. Procaccia, H. L. Swinney, and M. Thrasher, Europhys. Lett. **76**, 257 (2006).
[29] S. Li, J. S. Lowengrub, J. Fontana, and P. Palffy-Muhoray, Phys. Rev. Lett. **102**, 174501 (2009).
[30] A. Zosel, Colloid Polym. Sci. **263**, 541 (1985).
[31] H. Lakrout, P. Sergot, and C. Creton, J. Adhes. **69**, 307 (1999).
[32] B. A. Francis and R. G. Horn, J. Appl. Phys. **89**, 4167 (2005).
[33] D. Derks, A. Lindner, C. Creton, and D. Bonn, J. Appl. Phys. **93**, 1557 (2003).
[34] S. Poivet, F. Nallet, C. Gay, and P. Fabre, Europhys. Lett. **62**, 244 (2003).
[35] M. Tirumkudulu, W. B. Russel, and T. J. Huang, Phys. Fluids **15**, 1588 (2003).
[36] R. D. Welsh, M.Sc. thesis, Massachusetts Institute of Technology, 2001.
[37] J. A. Miranda, Phys. Rev. E **69**, 016311 (2004).
[38] J. A. Miranda, R. M. Oliveira, and D. P. Jackson, Phys. Rev. E **70**, 036311 (2004).
[39] S. Poivet, F. Nallet, C. Gay, J. Teisseire, and P. Fabre, Eur. Phys. J. E **15**, 97 (2004).
[40] Y. O. M. Abdelhaye, M. Chaouche, and H. Van Damme, Appl. Clay Sci. **42**, 163 (2008).
[41] S. A. Lira and J. A. Miranda, Phys. Rev. E **80**, 046313 (2009).
[42] Q. Barral, G. Ovarlez, X. Chateau, J. Boujlel, B. Rabideau, and P. Coussot, Soft Matter **6**, 1343 (2010).
[43] R. H. Ewoldt, P. Tourkine, G. H. McKinley, and A. E. Hosoi, Phys. Fluids **23**, 073104 (2011).
[44] E. O. Dias and J. A. Miranda, Phys. Rev. E **85**, 016312 (2012).
[45] E. O. Dias and J. A. Miranda, Phys. Rev. E **86**, 046322 (2012).
[46] P. G. Saffman and G. I. Taylor, Proc. R. Soc. London, Ser. A **245**, 312 (1958).
[47] J. A. Miranda and M. Widom, Int. J. Mod. Phys. B **12**, 931 (1998).
[48] H. Van Damme, in *The Fractal Approach to Heterogeneous Chemistry: Surfaces, Colloids, Polymers*, edited by D. Avnir (Wiley, Chichester, U.K., 1989), pp. 199–226.
[49] E. L. Decker, J. Ignés-Mullol, A. Baratt, and J. V. Maher, Phys. Rev. E **60**, 1767 (1999).
[50] A. Buka, P. Palffy-Muhoray, and Z. Racz, Phys. Rev. A **36**, 3984 (1987).
[51] H. Zhao and J. V. Maher, Phys. Rev. E **47**, 4278 (1993).
[52] L. Kondic, P. Palffy-Muhoray, and M. J. Shelley, Phys. Rev. E **54**, R4536 (1996).
[53] L. Kondic, M. J. Shelley, and P. Palffy-Muhoray, Phys. Rev. Lett. **80**, 1433 (1998).
[54] P. Fast, L. Kondic, M. J. Shelley, and P. Palffy-Muhoray, Phys. Fluids **13**, 1191 (2001).
[55] M. Constantin, M. Widom, and J. A. Miranda, Phys. Rev. E **67**, 026313 (2003).
[56] P. Fast and M. J. Shelley, J. Comput. Phys. **195**, 117 (2004).
[57] J. V. Fontana, S. A. Lira, and J. A. Miranda, Phys. Rev. E **87**, 013016 (2013).
[58] T. Podgorski, M. C. Sostarecz, S. Zorman, and A. Belmonte, Phys. Rev. E **76**, 016202 (2007).
[59] A. He, J. S. Lowengrub, and A. Belmonte, SIAM J. Appl. Math. **72**, 842 (2012).
[60] G. D. Carvalho, J. A. Miranda, and H. Gadêlha, Phys. Rev. E **88**, 053006 (2013).
[61] M. Zhao, A. Belmonte, S. Li, X. Li, and J. S. Lowengrub, J. Comput. Appl. Math. **307**, 394 (2016).
[62] J. V. Fontana, H. Gadêlha, and J. A. Miranda, Phys. Rev. E **93**, 033126 (2016).
[63] G. D. Carvalho, H. Gadêlha, and J. A. Miranda, Phys. Rev. E **89**, 053019 (2014).
[64] G. D. Carvalho, H. Gadêlha, and J. A. Miranda, Phys. Rev. E **90**, 063009 (2014).
[65] S. Li, J. S. Lowengrub, and P. H. Leo, J. Comput. Phys. **225**, 554 (2007).